Modelling the optical constants of cubic ZnS in the 0–20 eV spectral region

2003 J. Phys.: Condens. Matter 15 3717

(http://iopscience.iop.org/0953-8984/15/22/306)

INSTITUTE OF PHYSICS PUBLISHING JOURNAL OF PHYSICS: CONDENSED MATTER

J. Phys.: Condens. Matter **15** (2003) 3717–3730 PII: S0953-8984(03)56615-2

Modelling the optical constants of cubic ZnS in the 0–20 eV spectral region

Tomohide Tsuchiya, Shunji Ozaki and Sadao Adachi

Department of Electronic Engineering, Faculty of Engineering, Gunma University, Kiryu-shi, Gunma 376-8515, Japan

Received 20 November 2002
Published 23 May 2003
Online at stacks.iop.org/JPhysCM/15/3717

Abstract

We have analysed the complex dielectric-function spectra $\varepsilon(E) = \varepsilon_1(E) + i\varepsilon_2(E)$ of cubic (c-)ZnS in the full spectral range ($E = 0$–20 eV) using a classical harmonic oscillator and a simplified interband transition model. The experimental $\varepsilon(E)$ spectra reveal the reststrahlen band, distinct critical-point structures and cation d-band excitations in the spectra. The critical points are assigned to specific points in the Brillouin zone with the aid of the band-structure calculation. They are E_0 doublet at ∼3.8 eV; E_1 at ∼6.4 eV; E_2 at ∼7.0 eV; $E_2 + \delta$ at ∼7.4 eV; E_0' at ∼7.9 eV and E_1' at ∼9.4 eV. Excellent agreement is also achieved between the modelled and experimental $\varepsilon(E)$ spectra over the entire range of photon energies. The sum rules are used to extract more detailed information. The high-frequency and static dielectric constants of c-ZnS are determined to be $\varepsilon_\infty = 5.1$ and $\varepsilon_s = 8.0$, respectively. Dielectric-related optical constants, such as the complex refractive index, absorption coefficient and normal-incidence reflectivity, of c-ZnS are also presented.

1. Introduction

Zinc sulfide (ZnS) is the prototype II–VI semiconductor. Its cubic form (c-ZnS), which occurs naturally as a mineral, has given the name 'zincblende' to the crystal structure. The c-ZnS crystal is the primary candidate for ultraviolet optical devices as a consequence of its large bandgap energy, ∼3.8 eV at room temperature. Knowledge of the optical constants, such as the refractive indices and absorption coefficients, of semiconductors is especially important in the design and analysis of such optical devices. It is also of scientific interest to obtain the analytical expression for the optical response of semiconductors.

A number of models have been proposed in the literature to describe the optical response of semiconductors [1–8]. However, most of these models have been developed to describe the optical response only in a limited spectral region. In the long-wavelength limit, we observe a lattice absorption band, named the reststrahlen band, in heteropolar semiconductors [9]. Above the interband transition region, further weak structure is observed due to the onset of

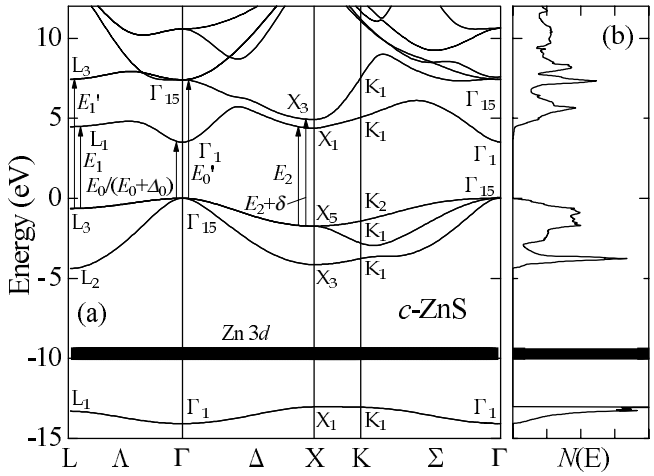

Figure 1. (a) Electronic energy-band structure and (b) DOS of c-ZnS as calculated by the EPM. The vertical arrows in (a) indicate the locations of several interband transitions in c-ZnS.

real transitions from atomic d-electron levels and/or plasma oscillations as collective excitations by the valence electrons [10].

In this paper we analyse the complex dielectric function $\varepsilon(E) = \varepsilon_1(E) + i\varepsilon_2(E)$ of c-ZnS in the full photon-energy range from 0 to 20 eV. The experimental $\varepsilon(E)$ data for c-ZnS are taken from tabulation in [11] ($T = 300$ K). The reststrahlen region ($E < 0.1$ eV) is analysed on the basis of a classical harmonic oscillator model and those above ∼0.1 eV are modelled by a simplified model of the interband transitions, namely, the model dielectric function (MDF) [1, 12]. The MDF includes the $E_0/(E_0 + \Delta_0)$, E_1, E_2, $E_2 + \delta$, E_0' and E_1' gaps as the main dispersion mechanisms. These gaps are assigned to specific points in the Brillouin zone by the aid of the band-structure calculation using an empirical pseudopotential method (EPM). The various optical sum rules provide a means of relating different physical properties without model fits to optical spectra [13]. Here we use the 'static-limit' sum rules to extract more detailed information on a zinc chalcogenide family, including c-ZnS.

2. Electronic energy-band structure of c-ZnS

We show in figure 1 the electronic energy-band structure and density-of-states (DOS) spectrum $N(E)$ for c-ZnS as calculated using the EPM. The spin–orbit interaction is not taken into account in the calculation. The vertical arrows in figure 1 indicate the locations of several interband transitions in c-ZnS.

We regarded the Zn 3d orbitals simply as core states. Note, however, that the cation d electrons play a significant role in II–VI and III–V semiconductors [14–17]. We, therefore, indicate the position of the Zn 3d band in figure 1. It is composed of five Zn 3d states. Due to the p–d hybridization with the anion p bands, the Zn 3d band is very narrow and exhibits very weak dispersion. The widths in energy of the Zn 3d band at the Γ point reported in [16] are 0.46 eV for c-ZnS, 0.37 eV for ZnSe and 0.21 eV for ZnTe, respectively.

In figure 1, the valence band consists of two subbands separated by ∼10 eV. The top anion p and bottom cation s valence shells have widths of about 4 and 1 eV, respectively. The spin–orbit interaction splits the Γ_{15} valence band into Γ_8 and Γ_7 (double-group notation, splitting energy Δ_0). The corresponding transitions at Γ are, respectively, labelled E_0 (Γ_8 (Γ_{15}) →

Γ_6 (Γ_1)) and $E_0 + \Delta_0$ (Γ_7 (Γ_{15}) $\rightarrow$ Γ_6 (Γ_1)). The Δ_0 value in c-ZnS is known to be very small, ∼70 meV [18, 19].

The spin–orbit interaction splits the L_3 valence band into $L_{4,5}$ and L_6 (splitting energy Δ_1). The corresponding transitions at or near L are, respectively, labelled E_1 ($L_{4,5}$ (L_3) $\rightarrow$ L_6 (L_1)) and $E_1 + \Delta_1$ (L_6 (L_3) $\rightarrow$ L_6 (L_1)). A value of $\Delta_1 = 50$ meV has been obtained theoretically [20], but at present no experimental data are available for c-ZnS. In the framework of the $\boldsymbol{k} \cdot \boldsymbol{p}$ method, the spin–orbit splitting Δ_0 at the Γ point is approximately one and a half times Δ_1 at the L point, namely, $\Delta_0/\Delta_1 \sim 3/2$ [21]. We found that many II–VI and III–V semiconductors obey the $\Delta_0/\Delta_1 \sim 3/2$ rule very well. It is, thus, reasonable to suppose that the Δ_1 value in c-ZnS is very small (a value of $\Delta_1 \sim 47$ meV is estimated from the $\Delta_0/\Delta_1 \sim 3/2$ rule).

The E_2 transitions in cubic semiconductors are expected to occur along the $\langle 110 \rangle$ (Σ) direction or near X (X_7 (X_5) $\rightarrow$ X_6 (X_1)). The E_1' transitions may occur at the L point ($L_{4,5}$ (L_3) $\rightarrow$ L_6 (L_3)). The higher transitions at or near Γ are labelled E_0' (Γ_8 (Γ_{15}) $\rightarrow$ Γ_7 (Γ_{15})).

The imaginary part of the dielectric function $\varepsilon_2(E)$ can be calculated from the electronic energy-band structure using the relation [22]

$$\varepsilon_2(E) = \frac{2e^2\hbar^4}{\pi m^2 E^2} \sum_{c,v} \int \left| \langle \boldsymbol{k}, c | \frac{\mathrm{d}}{\mathrm{d}\boldsymbol{x}} | \boldsymbol{k}, v \rangle \right|^2 \delta(E_{cv}(\boldsymbol{k}) - E)\, \mathrm{d}\boldsymbol{k} \tag{1}$$

where $|\boldsymbol{k}, c\rangle$ and $|\boldsymbol{k}, v\rangle$ represent the periodic parts of the wavefunctions of the conduction and valence bands, respectively, and $E_{cv}(\boldsymbol{k})$ is the energy difference between the conduction and valence bands. The integration is performed over the entire Brillouin zone with taking into account the $\boldsymbol{k}$-dependent momentum-matrix element [23].

The solid curve in figure 2(a) shows the calculated $\varepsilon_2(E)$ spectrum of c-ZnS from equation (1). Individual contributions to $\varepsilon_2(E)$ of the interband transitions in the specific parts of the Brillouin zone, Γ, L and X, are also shown in figure 2(a). The experimental $\varepsilon_2(E)$ spectrum for c-ZnS measured at $T = 300$ K is plotted in figure 2(b) by solid circles [11].

The calculated $\varepsilon_2(E)$ spectrum in figure 2(a) shows the main features of the measured curve; however, it does not show a quantitatively good fit. This is because we have not included a phenomenological relaxation time, i/τ, in the $\varepsilon_2(E)$ calculation to account for the lifetime-broadening effects. By choosing a finite τ value, it is principally possible to reproduce the strength (and width) of the experimentally measured ε_2 peaks. The excitonic effect should also be included to achieve better quantitative agreement with experiment.

The onset of optical absorption in the calculated $\varepsilon_2(E)$ spectrum of figure 2(a) occurs at ∼3.5 eV. It is clear that the most important contributions to the E_1 and E_1' peaks are due to the transitions at L. The nature of the E_2 structure is complicated, since it does not correspond to a single, well defined CP. It can be attributed to an accidental coincidence of saddle points at or near X and L in the Brillouin zone. The band-structure calculation also suggests the $E_2 + \delta$ CP at or near X (X_7 (X_5) $\rightarrow$ X_7 (X_3)). It should be noted that the splitting energy δ at the X point is zero in homopolar semiconductors (Si, Ge etc).

3. Model dielectric function

The relation between the energy-band structure and the imaginary part $\varepsilon_2(E)$ of the complex dielectric function in crystalline semiconductors can be given by [24]

$$\varepsilon_2(E) = \frac{4e^2\hbar^2}{\pi \mu^2 E^2} \int_S \mathrm{d}\boldsymbol{k}\, |P_{\mathrm{cv}}(\boldsymbol{k})|^2 \delta[E_c(\boldsymbol{k}_f) - E_v(\boldsymbol{k}_i) - E(\boldsymbol{k}_0)], \tag{2}$$

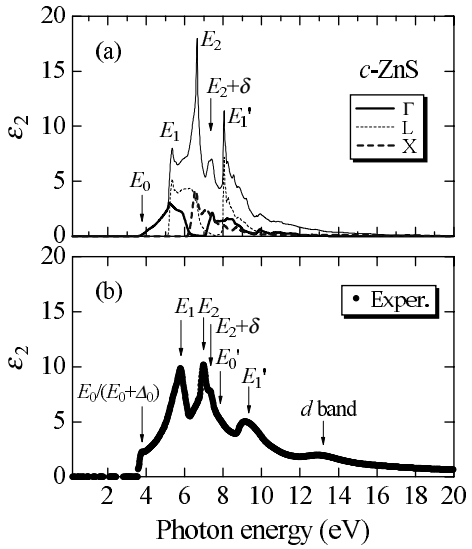

Figure 2. (a) $\varepsilon_2(E)$ spectrum of c-ZnS obtained from equation (1). Individual contributions to $\varepsilon_2(E)$ of the interband transitions in the specific parts of the Brillouin zone, Γ, L and X, are also shown. (b) $\varepsilon_2(E)$ spectrum of c-ZnS at $T = 300$ K taken from tabulation in [11]. The vertical arrows in (a) and (b) indicate the positions of several interband transitions and d-band excitations in c-ZnS.

where μ is the combined-DOS mass, $P_{cv}(\boldsymbol{k})$ is the momentum-matrix element between the valence- $E_v(\boldsymbol{k})$ and the conduction-band states $E_c(\boldsymbol{k})$ and $\boldsymbol{k} = \boldsymbol{k}_f - \boldsymbol{k}_i - \boldsymbol{k}_0$. Since the wavevector of the radiation $\boldsymbol{k}_0$ is usually very small compared to the dimension of the first Brillouin zone, we neglect it and obtain $\boldsymbol{k} \approx \boldsymbol{k}_f - \boldsymbol{k}_i$. The integration in equation (2) goes over the equal-energy-difference surface in $\boldsymbol{k}$ space defined by $E_c(\boldsymbol{k}_f) - E_v(\boldsymbol{k}_i) = E(\boldsymbol{k}_0)$.

In the MDF, equation (2) can be simply written as

$$\varepsilon_2(E) = \sum_{s=1}^{M} \frac{4e^2\hbar^2}{\pi(\mu^s)^2E^2}|P_{\mathrm{cv}}^s(\boldsymbol{k})|^2 J_{\mathrm{cv}}^s(E), \tag{3}$$

where $J_{\mathrm{cv}}^s(E)$ is the joint-DOS function of the sth interband CP. As can be understood from equation (3), the joint-DOS function mainly determines the interband contribution to $\varepsilon_2(E)$ and thus to the optical constants of solids. Analytical behaviours of $J_{\mathrm{cv}}^s(E)$ at various types of CP have been well defined [24].

The Kramers–Kronig (KK) relations assure that $\varepsilon_1(E)$ can be calculated at each photon energy if $\varepsilon_2(E)$ is known explicitly over the entire photon-energy range, and vice versa. These relations are given by

$$\varepsilon_1(E) = 1 + \frac{2}{\pi}\int_0^\infty \frac{E'\varepsilon_2(E')}{E'^2 - E^2}\,\mathrm{d}E', \tag{4a}$$

$$\varepsilon_2(E) = -\frac{2E}{\pi}\int_0^\infty \frac{\varepsilon_1(E')}{E'^2 - E^2}\,\mathrm{d}E'. \tag{4b}$$

In the following, we summarize the MDFs for CP of each energy gap [12]. Combining all these contributions, one can obtain the spectral dependence of $\varepsilon(E)$ of the material in the entire range of photon energies.

The E_0 and $E_0 + \Delta_0$ gaps are of the three-dimensional (3D) M_0 CPs and occur in c-ZnS at ∼3.8 eV. The contributions of these gaps to $\varepsilon(E)$ are given by

$$\varepsilon(E) = AE_0^{-3/2}\left[f(\chi_0) + \frac{1}{2}\left(\frac{E_0}{E_0+\Delta_0}\right)^{3/2} f(\chi_{so})\right], \tag{5}$$

with

$$f(\chi_0) = \chi_0^{-2}[2 - (1+\chi_0)^{1/2} - (1-\chi_0)^{1/2}], \tag{6a}$$

$$f(\chi_{so}) = \chi_{so}^{-2}[2 - (1+\chi_{so})^{1/2} - (1-\chi_{so})^{1/2}], \tag{6b}$$

$$\chi_0 = \frac{E + \mathrm{i}\Gamma}{E_0}, \tag{7a}$$

$$\chi_{so} = \frac{E + \mathrm{i}\Gamma}{E_0 + \Delta_0}. \tag{7b}$$

In equations (5)–(7), A and Γ are, respectively, the strength and broadening parameters of the E_0 and $E_0 + \Delta_0$ CPs.

The discrete series of excitons at the E_0 and $E_0 + \Delta_0$ edges can be simply written as

$$\varepsilon(E) = \sum_{n=1}^{\infty} \frac{A_{0x}}{n^3}\left[\frac{1}{[E_0 - (G_0/n^2)]^2 - E^2 - \mathrm{i}2E\Gamma} + \frac{1}{2}\frac{1}{[E_0 + \Delta_0 - (G_0/n^2)]^2 - E^2 - \mathrm{i}2E\Gamma}\right], \tag{8}$$

where A_{0x} is the exciton strength parameter and G_0 is the 3D-exciton Rydberg energy.

The E_1 and $E_1 + \Delta_1$ CPs are assumed to be of the two-dimensional (2D) M_0 type and occur in c-ZnS at ∼6.5 eV. The contributions to $\varepsilon(E)$ of these CPs are given by

$$\varepsilon(E) = -B_1\chi_{1d}^{-2}\ln(1-\chi_{1d}^2) - B_2\chi_{1sd}^{-2}\ln(1-\chi_{1sd}^2), \tag{9}$$

$$\varepsilon(E) = \sum_{n=1}^{\infty} \frac{1}{(2n-1)^3}\left[\frac{B_{1x}}{(E_1 - [4G_1/(2n-1)^2])^2 - E^2 - \mathrm{i}2E\Gamma} + \frac{B_{2x}}{(E_1 + \Delta_1 - [4G_1/(2n-1)^2])^2 - E^2 - \mathrm{i}2E\Gamma}\right], \tag{10}$$

with

$$\chi_{1d} = \frac{E + \mathrm{i}\Gamma}{E_1}, \tag{11a}$$

$$\chi_{1sd} = \frac{E + \mathrm{i}\Gamma}{E_1 + \Delta_1}, \tag{11b}$$

where B_i (B_{ix}) and Γ are the one-electron (2D-exciton) strength parameter and broadening energy of the E_1 and $E_1 + \Delta_1$ transitions, respectively, and G_1 is the 2D-exciton Rydberg energy. Because of the small Δ_1 value of c-ZnS, we neglect the contribution to $\varepsilon(E)$ of the $E_1 + \Delta_1$ transitions.

The E_2 transitions in c-ZnS occur at ∼7 eV and are characterized by a damped harmonic oscillator (DHO). The contribution to $\varepsilon(E)$ of this CP is given by

$$\varepsilon(E) = \frac{C}{(1-\chi_2^2) - \mathrm{i}\chi_2\gamma}, \tag{12}$$

with

$$\chi_2 = \frac{E}{E_2}, \tag{13}$$

where C and γ are the nondimensional strength and broadening parameters of the DHO, respectively. The higher-lying CPs, such as $E_2 + \delta$, E_0' and E_1', and d-band excitations are also found to be well characterized by the DHO model.

The MDFs presume a broadening mechanism of Lorentzian type. If Gaussian broadening is assumed, the dielectric function cannot be expressed as in a closed analytical form. However, the substitution of the quantity

$$\Gamma^* = \Gamma \exp\left[-\alpha\left(\frac{E - E_g}{\Gamma}\right)^2\right] \tag{14}$$

for Γ (γ) in equations (5)–(12) leads to analytical functions which have been shown to closely mimic the numerical results for the Gaussian case, for appropriate values of α [5, 25, 26].

By putting $\alpha = 0$, the causality, linearity, reality and Kramers–Kronig requirements, compulsory properties of $\varepsilon(E)$, are satisfied automatically; however, this is not the case if Gaussian-like broadening ($\alpha \neq 0$) is assumed. This can be easily understood from a failure in the causality of the dielectric response

$$\begin{aligned} \varepsilon_1(E) &= \varepsilon_1(-E) \\ -\varepsilon_2(E) &= \varepsilon_2(-E), \end{aligned} \tag{15}$$

if one puts the Gaussian-like expression equation (14) into the MDFs or any arbitrary function that can be used as a model dielectric function. The fact has been proved more clearly in the optical dispersion analysis of amorphous semiconductors [27]. Thus, users of the MDFs with equation (14) should be aware of this inconsistency and check self-consistency of the dielectric function between the real and imaginary parts. In the following analysis, we assume Lorentzian-type broadening ($\alpha = 0$).

4. Results and discussion

The fits with our model to the experimental $\varepsilon(E)$ spectra of c-ZnS are shown in figure 3. The experimental data are taken from tabulation in [11]. They were compiled from [28] for $E \leqslant 0.07$ eV, from [29] for $0.103 \leqslant E \leqslant 0.413$ eV, from [30] for $0.516 \leqslant E \leqslant 2.754$ eV, from [31] for $2.75 \leqslant E \leqslant 5.4$ eV and from [32] for $5.7 \leqslant E \leqslant 20$ eV.

Below the reststrahlen range in optical spectra ($E < 0.03$ eV), the real part of the dielectric constant asymptotically approaches the static or low-frequency dielectric constant ε_s. The optical constant concerning the reststrahlen–near-infrared range is called the high-frequency or optical dielectric constant ε_∞. The high-frequency dielectric constant, thus, is measured for frequencies well above the long-wavelength optical phonon frequency but below the fundamental absorption edge.

The complex dielectric function $\varepsilon(E)$ in the long-wavelength limit can be generally explained by a classical Lorentz oscillator model [9]

$$\varepsilon(\omega) = \varepsilon_\infty\left(1 + \frac{\omega_{LO}^2 - \omega_{TO}^2}{\omega_{TO}^2 - \omega^2 - i\omega\gamma_T}\right), \tag{16}$$

where ω_{LO} and ω_{TO} are the transverse optical (TO) and longitudinal optical (LO) phonon frequencies, respectively, and γ_T is the damping constant of the optical phonons. Note that the optical dielectric contribution ε_∞ in equation (16) mainly arises from the interband transitions described in section 3. In order to avoid an overaccounting of this contribution, we express the reststrahlen contribution to $\varepsilon(E)$ as

$$\varepsilon(\omega) = \frac{\varepsilon_\infty(\omega_{LO}^2 - \omega_{TO}^2)}{\omega_{TO}^2 - \omega^2 - i\omega\gamma_T} = \frac{S}{\omega_{TO}^2 - \omega^2 - i\omega\gamma_T}, \tag{17}$$

where $S \equiv \varepsilon_\infty(\omega_{LO}^2 - \omega_{TO}^2)$ is the reststrahlen-band strength parameter.

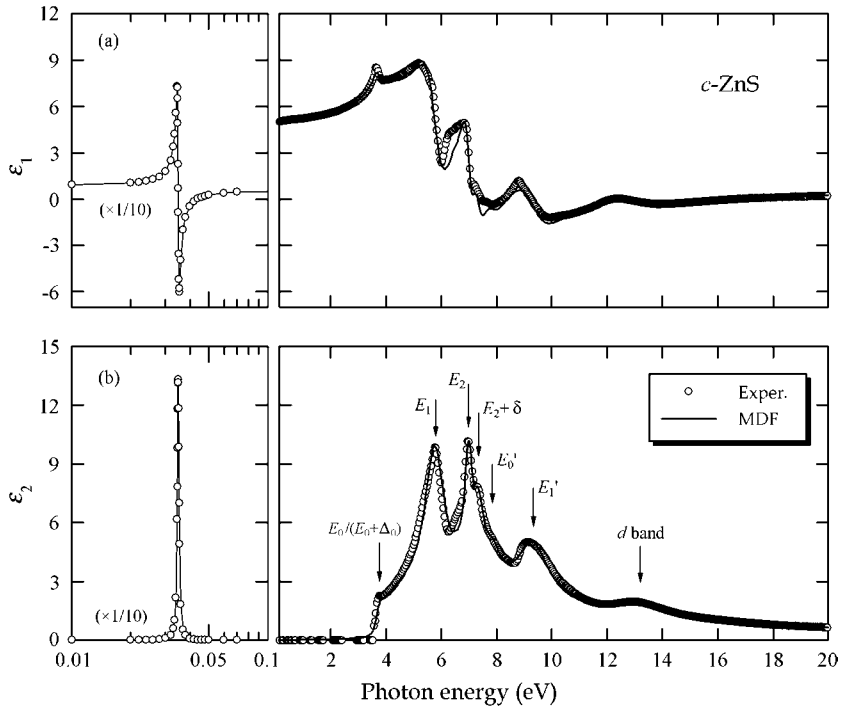

Figure 3. MDF fit to $\varepsilon(E)$ for c-ZnS. The solid curves are obtained from the sum of equations (5), (8)–(10), (12) and (17) and $\varepsilon_{1\infty}$. The experimental data are taken from [11]. The fit-determined MDF parameters are listed in table 1. The vertical arrows indicate the positions of several interband transitions and d-band excitations in c-ZnS.

The solid curves in figure 3 are obtained from the sum of equations (5), (8)–(10), (12) and (17). The best-fit parameters are listed in table 1. The experimental $\varepsilon_1(E)$ are usually somewhat larger than our calculation model. In order to improve the fit, therefore, we considered an addition term, $\varepsilon_{1\infty}$, to ε_1. This term is assumed to be constant and may arise from higher-energy excitations (e.g. core excitons).

The MDF requires three fitting parameters (CP energy, strength and broadening parameters) per CP. The CP energies determined here are in reasonable agreement with those reported in [33]. The 3D-exciton Rydberg energy G_0 reported for c-ZnS varies from 34 to 39 meV [34–37]. We used a value of $G_0 = 34$ meV [35, 37]. Neither experimental nor theoretical value on the 2D-exciton Rydberg parameter G_1 has been reported for c-ZnS to date. The 3D and 2D Rydberg values reported for ZnTe are $G_0 \sim 10$ meV and $G_1 \sim 47.5$ meV, respectively [38]. Keeping the ratio $G_1/G_0 = 4.75$ and inserting a value of $G_0 \sim 34$ meV, we obtain G_1 value for c-ZnS to be ∼162 meV.

Using such MDF parameters, we can obtain reasonable agreement between the MDF-calculated and experimental $\varepsilon_2(E)$ spectra over the entire range of photon energies (figure 3(b)). We must note, however, that the calculated $\varepsilon_1(E)$ spectrum shows no good agreement with the experimental data in the 6–8 eV spectral region. The data in this region were deduced from fundamental reflectivity by performing KK analysis [32]. The experimental ε_1 and ε_2 spectra must satisfy the KK self-consistency. As mentioned before, our MDF fully satisfies the KK requirements. Thus, if the experimental $\varepsilon_2(E)$ spectrum agrees satisfactorily well with the MDF-calculated spectrum, as in figure 3(b), then the same agreement must be achieved

Table 1. Parameter values used in the calculation of $\varepsilon(E)$ for c-ZnS.

Parameter	Value
ω_{TO} (cm^{-1})	281
S (10^5 cm^{-2})	2.56
γ_T (cm^{-1})	6.8
E_0 (eV)	3.77
$E_0 + \Delta_0$ (eV)	3.84
A ($eV^{1.5}$)	35.5
Γ (eV)	0.12
G_0 (eV)	0.034
A_{0x} (eV^2)	0.80
Γ (eV)	0.12
E_1 (eV)	6.43
B_1	0.25
Γ (eV)	0.44
G_1 (eV)	0.162
B_{1x} (eV^2)	37.0
Γ (eV)	0.44
E_2 (eV)	6.99
C	0.29
γ (eV)	0.05
$E_2 + \delta$ (eV)	7.36
C	0.18
γ	0.06
E_0' (eV)	7.86
C	0.13
γ	0.09
E_1' (eV)	9.34
C	0.44
γ	0.15
d band (eV)	13.2
C	0.10
γ	0.15
$\varepsilon_{1\infty}$	0.39

between the experimental and MDF-calculated $\varepsilon_1(E)$ spectra. It is, thus, considered that the experimental $\varepsilon(E)$ values in the 6–8 eV spectral region are doubtful. It is not easy to accurately measure the reflectivity spectrum. Small differences in reflectivity can result in large difference in ε. Further, ε values from reflectivity measurements are based on an indirect determination technique with several assumptions and approximations.

The energy-loss function defined by $-\operatorname{Im}\varepsilon(E)^{-1}$ involves both one-electron excitations and many-body resonances, such as excitons or plasmons. This is illustrated in figure 4 where the experimental $\operatorname{Im}\varepsilon(E) = \varepsilon_2(E)$ and $-\operatorname{Im}\varepsilon(E)^{-1}$ are plotted by solid and open circles, respectively. The solid curves indicate the MDF-calculated $\operatorname{Im}\varepsilon(E)$ and $-\operatorname{Im}\varepsilon(E)^{-1}$ spectra. Most of the structures observed below ~10 eV in $\operatorname{Im}\varepsilon(E)$ and $-\operatorname{Im}\varepsilon(E)^{-1}$ are due to the interband transitions. The structure at ~12–13 eV is due to the d-band excitations (i.e., transitions from the Zn 3d band into the conduction band). This structure can be characterized well by the DHO (figure 3). Around 20 eV a further structure is observed as a broad peak in the energy-loss spectrum $-\operatorname{Im}\varepsilon(E)^{-1}$. In this so-called plasma region the valence electrons can behave like free particles and take part in collective oscillations.

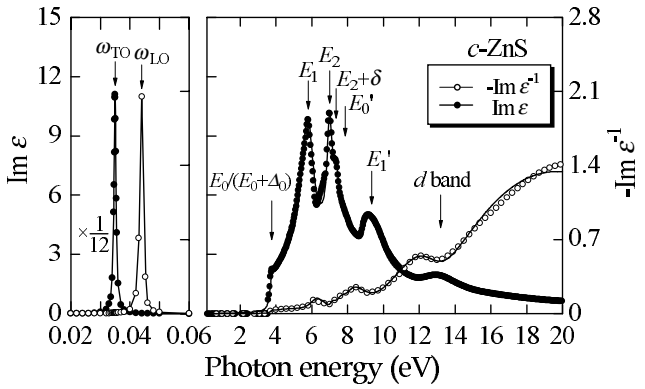

Figure 4. Experimental $\operatorname{Im}\varepsilon(E) = \varepsilon_2(E)$ and $-\operatorname{Im}\varepsilon(E)^{-1}$ spectra for c-ZnS. The solid curves represent the MDF-calculated $\operatorname{Im}\varepsilon(E)$ and $-\operatorname{Im}\varepsilon(E)^{-1}$ spectra. The vertical arrows indicate the positions of several interband transitions and d-band excitations in c-ZnS. The positions of the TO and LO phonon frequencies are also indicated by ω_{TO} and ω_{LO}, respectively.

In the reststrahlen region, the loss function $-\operatorname{Im}\varepsilon(E)^{-1}$ and $\operatorname{Im}\varepsilon(E)$ can be given by

$$-\operatorname{Im}\varepsilon(\omega)^{-1} = \frac{(\varepsilon_\infty^{-1} - \varepsilon_s^{-1})\omega_{\mathrm{LO}}^2\omega\gamma_{\mathrm{T}}}{(\omega_{\mathrm{LO}}^2 - \omega^2)^2 + \omega^2\gamma_{\mathrm{T}}^2}, \tag{18a}$$

$$\operatorname{Im}\varepsilon(\omega) = \frac{(\varepsilon_s - \varepsilon_\infty)\omega_{\mathrm{TO}}^2\omega\gamma_{\mathrm{T}}}{(\omega_{\mathrm{TO}}^2 - \omega^2)^2 + \omega^2\gamma_{\mathrm{T}}^2}, \tag{18b}$$

which become for $\omega \sim \omega_{\mathrm{LO}}$ and $\omega \sim \omega_{\mathrm{TO}}$

$$-\operatorname{Im}\varepsilon(\omega)^{-1} = \frac{(\varepsilon_\infty^{-1} - \varepsilon_s^{-1})\omega_{\mathrm{LO}}\gamma_{\mathrm{T}}}{4(\omega_{\mathrm{LO}} - \omega)^2 + \gamma_{\mathrm{T}}^2}, \tag{19a}$$

$$\operatorname{Im}\varepsilon(\omega) = \frac{(\varepsilon_s - \varepsilon_\infty)\omega_{\mathrm{TO}}\gamma_{\mathrm{T}}}{4(\omega_{\mathrm{TO}} - \omega)^2 + \gamma_{\mathrm{T}}^2}. \tag{19b}$$

Hence, the maxima in $-\operatorname{Im}\varepsilon(\omega)^{-1}$ and $\operatorname{Im}\varepsilon(E)$ determine the optical phonon frequencies ω_{LO} and ω_{TO}, respectively, as demonstrated in figure 4. The optical phonon frequencies determined in figure 4 are $\omega_{\mathrm{LO}} = 352\ \mathrm{cm}^{-1}$ and $\omega_{\mathrm{TO}} = 281\ \mathrm{cm}^{-1}$.

A number of useful relations can be derived which relate the real and imaginary parts of the dielectric function and optical constants [13]. The so-called dispersion relations and sum rules have been extremely valuable in analysing and testing optical-constant data. Let us consider the following sum rules [10]:

$$n_{eff} = \frac{2\pi m\varepsilon_0}{Ne^2h^2}\int_0^{E_{\mathrm{M}}} E\varepsilon_2(E)\,\mathrm{d}E, \tag{20}$$

$$\varepsilon_1(0)_{eff} = 1 + \frac{2}{\pi}\int_0^{E_{\mathrm{M}}} \frac{\varepsilon_2(E)}{E}\,\mathrm{d}E, \tag{21}$$

where N is the number of atoms per m^3. Figures 5(a) and (b) plot n_{eff} and $\varepsilon_1(0)_{eff}$ versus E_M for c-ZnS, respectively. For comparison, those for ZnSe, ZnTe and Si are plotted. The numerical $\varepsilon_2(E)$ values for these semiconductors are taken from [11].

Equation (20) relates n_{eff}, the effective number of valence electrons per atom taking part in optical transitions in the range of photon energies up to E_M, to $\varepsilon_2(E)$. If transitions involving the valence electrons are well separated in energy from absorption associated with

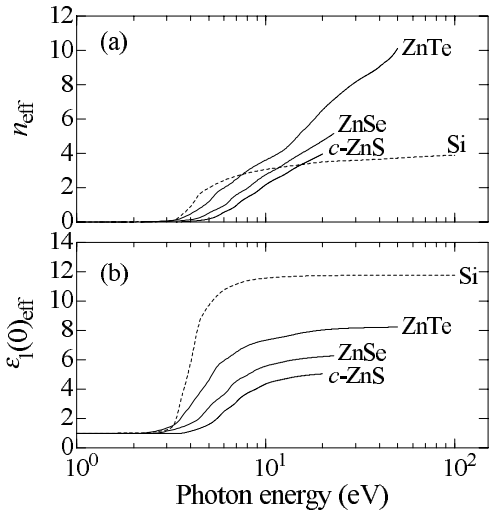

Figure 5. (a) n_{eff} and (b) $\varepsilon_1(0)_{eff}$ for c-ZnS. For comparison, those for ZnSe, ZnTe and Si are also plotted. The numerical $\varepsilon_2(E)$ values used in the calculations for these semiconductors are taken from tabulation in [11].

core electrons, then this integral should behave in a very obvious way. For example, in the tetrahedrally bonded materials the number of valence electrons per atom is four, irrespective of the nature of bonding, and thus n_{eff} will approach a value of four at sufficiently large photon energy. The plot of Si is just the case for this. By contrast, n_{eff} values for Zn chalcogenides extend appreciably above four. The increase above four is due to the d-band excitations (i.e., real transitions between the filled Zn 3d states, lying below the valence band, and empty conduction band). The d-band state is absent in Si.

Equation (20) predicts further increase in n_{eff} when E_M approaches the d-band excitations. If the cation d band is sufficiently well separated from the anion p band, n_{eff} will saturate at a value of nine electrons per atom for E_M such that the f-sum for the cation d band is exhausted. This is not the case in the Zn chalcogenides. The E_M values at which n_{eff} values get beyond four are 20.5, 15.5 and 11.7 eV for c-ZnS, ZnSe and ZnTe, respectively. We can, therefore, suppose stronger p (anion)–d (Zn) hybridization occurring in ZnTe than in c-ZnS.

From the tendency toward saturation for $\varepsilon_1(0)_{eff}$ at photon energies below ∼10 eV, it is evident that strong interband transitions below this energy are mainly responsible for the value of the optical dielectric constant. In crystalline material, the real part of the dielectric function $\varepsilon_1(0)_{eff}$ approaches the optical dielectric constant, ε_∞, as $E_M \to \infty$ eV. Measurements of the optical dielectric constant ε_∞ for c-ZnS have yielded widely different values ranging from 4.7 to 5.7 (see [28, 39–41]; table 2). The curves in figure 5(b) saturate at a value of $\varepsilon_\infty \sim 5.1$ for c-ZnS, ∼6.3 for ZnSe, ∼8.3 for ZnTe and ∼11.8 for Si. The c-ZnS value obtained here is exact agreement with the average value of the literature data (∼5.1, table 2). The ε_s and ε_∞ are related to the optical phonon frequencies, $\omega_{\rm LO}$ and $\omega_{\rm TO}$, by the generalized Lyddane–Sachs–Teller relation

$$\frac{\varepsilon_s}{\varepsilon_\infty} = \left(\frac{\omega_{\rm LO}}{\omega_{\rm TO}}\right)^2. \tag{22}$$

Introducing $\omega_{\rm LO} = 352$ cm^{-1}, $\omega_{\rm TO} = 281$ cm^{-1}, and $\varepsilon_\infty = 5.1$ into equation (22), we obtain 8.0 for the value of ε_s.

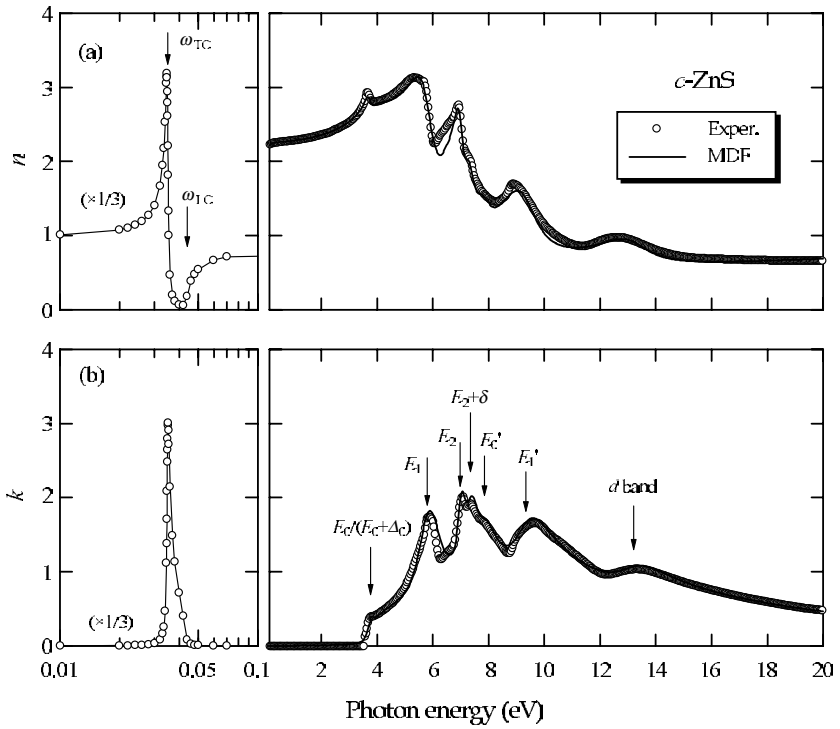

Figure 6. MDF-calculated $n(E)$ and $k(E)$ spectra for c-ZnS. The solid curves are obtained from equation (23) for $n(E)$ and from equation (24) for $k(E)$, respectively. The open circles show the experimental data taken from tabulation in [11]. The vertical arrows indicate the positions of several interband transitions and d-band excitations in c-ZnS. The positions of the TO and LO phonon frequencies are also indicated by ω_{TO} and ω_{LO}, respectively.

Table 2. Static (ε_s) and high-frequency dielectric constants (ε_∞) of c-ZnS.

ε_s	ε_∞	T (K)	References
8.9	5.7	300	[28]
8.14		77	[39]
8.37		298	[39]
8.04	4.9	2	[40]
8.10	4.8	80	[40]
8.34	4.7	300	[40]
8.1		75.6	[41]
8.3	5.20	300	[41]
8.0	5.1	300	Present study

Optical spectra, such as the complex refractive index $n^*(E) = n(E) + \mathrm{i}k(E)$, absorption coefficient $\alpha(E)$ and normal-incidence reflectivity $R(E)$, can be calculated from the present study, since they are directly related to the complex dielectric function $\varepsilon(E)$. The real refractive index $n(E)$ and extinction coefficient $k(E)$ can now be written as

$$n(E) = \left(\frac{[\varepsilon_1(E)^2 + \varepsilon_2(E)^2]^{1/2} + \varepsilon_1(E)}{2} \right)^{1/2}, \tag{23}$$

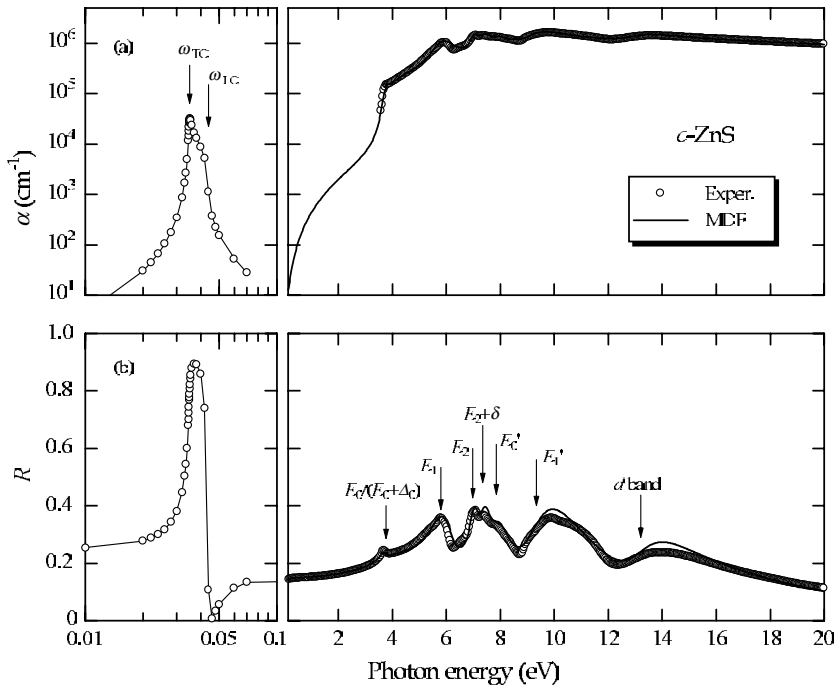

Figure 7. MDF-calculated $\alpha(E)$ and $R(E)$ spectra for c-ZnS. The solid curves are obtained from equation (25) for $\alpha(E)$ and from equation (26) for $R(E)$, respectively. The open circles show the experimental data taken from tabulation in [11]. The vertical arrows indicate the positions of several interband transitions and d-band excitations in c-ZnS. The positions of the TO and LO phonon frequencies are also indicated by ω_{TO} and ω_{LO}, respectively.

$$k(E) = \left(\frac{[\varepsilon_1(E)^2 + \varepsilon_2(E)^2]^{1/2} - \varepsilon_1(E)}{2} \right)^{1/2}. \tag{24}$$

The MDF-calculated $n(E)$ and $k(E)$ spectra for c-ZnS are shown in figure 6. The solid curves are obtained from equations (23) and (24). The open circles represent the experimental data. The strong peaks seen in n at $E \sim 3$–10 eV correspond to the E_0, E_1, E_2 and E_1' transitions. The peak due to the d-band excitations is also clearly found at $E \sim 13$ eV. In the reststrahlen region ($E < 0.1$ eV), the refractive index is determined to be $n_\infty \sim (\varepsilon_\infty)^{1/2} \sim 2.2$. For $k(E)$, the strongest peak at $E \sim 7$ eV is related mainly to the E_2 and $E_2 + \delta$ transitions. The k above $\sim$3.8 eV is associated with the onset of the $E_0/(E_0 + \Delta_0)$-gap 3D-exciton transitions and that at $E \sim 6$ eV is dominated by the 2D-exciton (E_1) transitions.

The absorption coefficient $\alpha(E)$ and normal-incidence reflectivity $R(E)$ can be given by

$$\alpha(E) = \frac{4\pi}{\lambda} k(E), \tag{25}$$

$$R(E) = \frac{[n(E) - 1]^2 + k(E)^2}{[n(E) + 1]^2 + k(E)^2}, \tag{26}$$

where λ is the light wavelength in the vacuum.

The MDF-calculated $\alpha(E)$ and $R(E)$ spectra for c-ZnS are shown in figure 7. The solid lines show the calculated results of equations (25) and (26) with $n(E)$ and $k(E)$ from equations (23) and (24), respectively. The open circles represent the experimental data taken from [11]. In figure 7(a), $\alpha(E)$ shows a saturated value of $\sim 1 \times 10^6$ cm^{-1} at $E > 6$ eV. The

reststrahlen α peak value is about 3×10^4 cm^{-1} at $E \sim 0.035$ eV. The $R(E)$ spectrum reveals the various CPs and d-band excitations in the spectrum. It is evident from figures 6 and 7 that our MDF calculation reproduces the peculiar optical-constant spectra of c-ZnS over the entire range of photon energies (0–20 eV).

5. Conclusions

We have analysed the real (ε_1) and imaginary parts (ε_2) of the complex dielectric function of c-ZnS in the 0–20 eV photon-energy range. The analysed $\varepsilon(E)$ spectra reveal the lattice absorption band, distinct CP structures and cation core-level excitations in the spectra. These data are analysed using a classical harmonic oscillator and a simplified interband transition model. The band-structure calculation is also performed to assign such optical transitions to specific points in the Brillouin zone. Excellent agreement is achieved between the MDF-calculated and experimental $\varepsilon(E)$ spectra over the entire range of photon energies. Dielectric-related optical constants, such as the complex refractive index, absorption coefficient and normal-incidence reflectivity, of c-ZnS have also been presented.

References

[1] Adachi S 1987 *Phys. Rev.* B **35** 7475
[2] Forouhi A R and Bloomer I 1988 *Phys. Rev.* B **38** 1865
[3] Jenkins D W 1990 *J. Appl. Phys.* **68** 1848
[4] Terry F L Jr 1991 *J. Appl. Phys.* **70** 409
[5] Kim C C, Garland J W, Avad H and Raccah P M 1992 *Phys. Rev.* B **45** 11749
[6] Lin C-H and Meese J M 1993 *J. Appl. Phys.* **74** 6341
[7] Rakić A D and Majewski M L 1996 *J. Appl. Phys.* **80** 5909
[8] Djurišić A B, Rakić A D, Kwok P C K, Li E H, Majewski M L and Elazar J M 1999 *J. Appl. Phys.* **86** 445
[9] Balkanski M 1972 *Optical Properties of Solids* ed F Abelès (Amsterdam: North-Holland) p 529
[10] Philipp H R and Ehrenreich H 1963 *Phys. Rev.* **129** 1550
[11] Adachi S 1999 *Optical Constants of Crystalline and Amorphous Semiconductors: Numerical Data and Graphical Information* (Boston, MA: Kluwer)
[12] Adachi S 1999 *Optical Properties of Crystalline and Amorphous Semiconductors: Materials and Fundamental Principles* (Boston, MA: Kluwer)
[13] Smith D Y 1985 *Handbook of Optical Constants of Solids* ed E D Palik (Orlando, FL: Academic) p 35
[14] Wei S-H and Zunger A 1988 *Phys. Rev.* B **37** 8958
[15] Wright A F and Nelson J S 1994 *Phys. Rev.* B **50** 2159
[16] Lee Gun-Do, Lee M H and Ihm J 1995 *Phys. Rev.* B **52** 1459
[17] Rohlfing M, Krüger P and Pollmann J 1998 *Phys. Rev.* B **57** 6485
[18] Matatagui E, Thompson A G and Cardona M 1968 *Phys. Rev.* **176** 950
[19] Fernández M, Prete P, Lovergine N, Mancini A M, Cingolani R, Vasanelli L and Perrone M R 1997 *Phys. Rev.* B **55** 7660
[20] Ekpenuma S N and Myles C W 1990 *J. Phys. Chem. Solids* **51** 93
[21] Cardona M, Shaklee K L and Pollak F H 1967 *Phys. Rev.* **154** 696
[22] Au-Yang M Y and Cohen M L 1969 *Phys. Rev.* **178** 1279
[23] Gilat G and Bharatiya N R 1975 *Phys. Rev.* B **12** 3479
[24] See, for instance,
Harbake G 1972 *Optical Properties of Solids* ed F Abelès (Amsterdam: North-Holland) p 21
[25] Kim C C, Garland J W and Raccah P M 1993 *Phys. Rev.* B **47** 1876
[26] Kim C C and Sivananthan S 1995 *J. Appl. Phys.* **78** 4003
[27] Mori H and Adachi S 2003 *Japan. J. Appl. Phys.* **42** 58
[28] Manabe A, Mitsuishi A and Yoshinaga H 1967 *Japan. J. Appl. Phys.* **6** 593
[29] *Eastman Kodak Publication* U-72 1972 (Rochester, NY)
[30] Bond W L 1965 *J. Appl. Phys.* **36** 1674
[31] Ozaki S and Adachi S 1993 *Japan. J. Appl. Phys.* **32** 5008

[32] Cardona M and Harbeke G 1965 *Phys. Rev.* **137** A1467
[33] Hellwege K-H and Madelung O (ed) 1982 *Numerical Data and Functional Relationships in Science and Technology (Landolt–Börnstein New Series)* Group III vol 17 a (Berlin: Springer)
[34] Taguchi T, Yokogawa T and Yamashita H 1984 *Solid State Commun.* **49** 55
[35] Mang A, Reimann K, Rübenacke St and Steube M 1996 *Phys. Rev.* B **53** 16283
[36] Fernández M, Prete P, Lovergine N, Mancini A M, Cingolani R, Vasanelli L and Perrone M R 1997 *Phys. Rev.* B **55** 7660
[37] Pässler R, Griebl E, Riepl H, Lautner G, Bauer S, Preis H, Gebhardt W, Buda B, As D J, Schikora D, Lischka K, Papagelis K and Ves S 1999 *J. Appl. Phys.* **86** 4403
[38] Adachi S and Sato K 1992 *Japan. J. Appl. Phys.* **31** 3907
[39] Berlincourt D, Jaffe H and Shiozawa L R 1963 *Phys. Rev.* **129** 1009
[40] Hattori T, Homma Y, Mitsuishi A and Tacke M 1973 *Opt. Commun.* **7** 229
[41] Samara G A 1983 *Phys. Rev.* B **27** 3494